Supplementary Materials for: Interface pinning causes the hysteresis of the hydride transformation in binary metal hydrides

Nicholas J. Weadock,[1] Peter W. Voorhees,[2,3] and Brent Fultz[1]

[1]*Department of Applied Physics and Materials Science*
California Institute of Technology, Pasadena, CA, USA
[2]*Department of Materials Science and Engineering*
Northwestern University, Evanston, IL, USA
[3]*Engineering Sciences and Applied Mathematics*
Northwestern University, Evanston, IL, USA

(Dated: December 10, 2020)

I. ELECTRON MICROGRAPHS OF BULK PALLADIUM

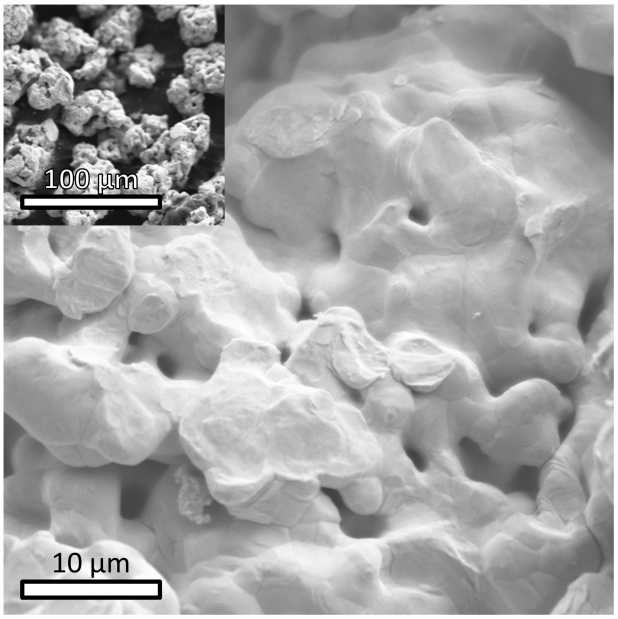

FIG. 1. Scanning electron micrograph of a bulk Pd particle consisting of coalesced grains. The inset shows the scale of individual particles; inset scale bar is 100μm.

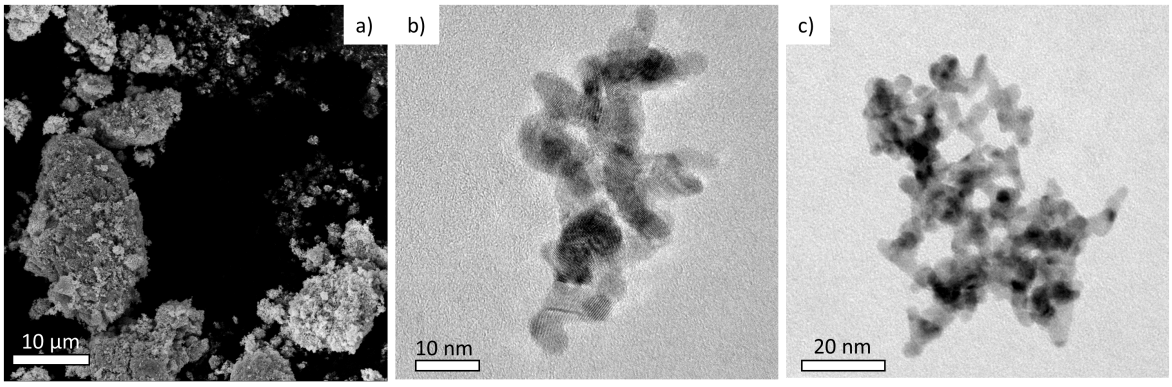

FIG. 2. Additional electron micrographs of the Pd nanopowder. a) Scanning electron micrograph of the as-received nanopowder, showing significant agglomeration. Transmission electron micrographs of the sonicated nanopowder in b) and c) show smaller porous agglomerates of nanocrystallites.

II. COMPARISON OF PRESSURE-COMPOSITION ISOTHERM MEASUREMENTS IN A SIEVERT'S APPARATUS AND *IN-SITU* X-RAY DIFFRACTION SAMPLE CHAMBER

Pressure composition isotherms were measured during the *in-situ* x-ray diffraction studies for bulk and nanocrystalline Pd samples. Figure 3 below compares the *in-situ* and Sievert's pressure composition isotherms measured for bulk (a) and nanocrystalline (b) Pd. For both samples the plateau pressures for absorption and desorption are slightly greater in the *in-situ* setup than those measured for with the Sievert's apparatus. Hysteresis values, however, the same for both types of measurements.

We attribute the pressure discrepancy to the different heating stages in the equipment. On the Sievert's apparatus, a stainless steel reactor is completely enclosed by a large aluminum block wrapped in a band heater. Several type K thermocouples are used for redundant temperature measurement and PID control. The *in-situ* heating stage consists of a small aluminum plate with a milled vertical sample channel. A 40 watt power resistor is affixed to the back of the plate opposite the sample channel. Due to the restrictive geometry of the hydrogen environment chamber feedthrough, only a single type K thermocouple is used for both monitoring and PID control. This thermocouple is inserted into the aluminum plate below both the sample channel and heater, which could result in an artificially high temperature at the sample. We use the van't Hoff equation and experimentally determined

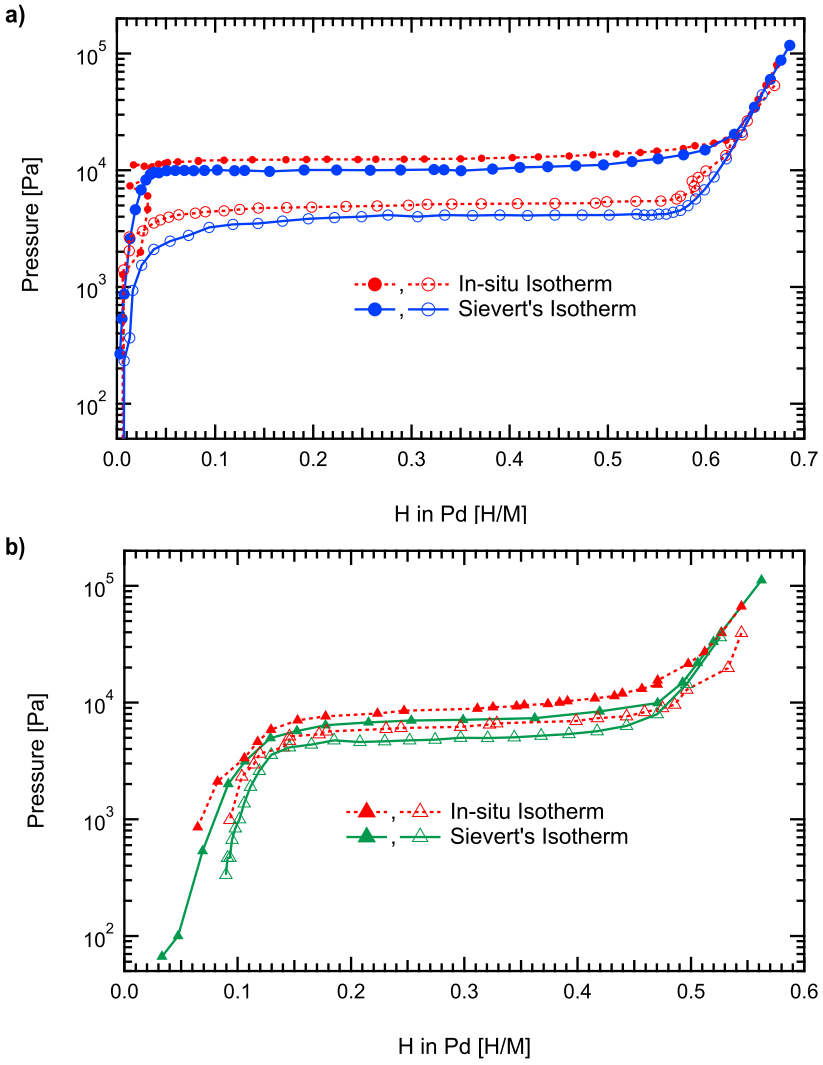

FIG. 3. Comparison of pressure-composition isotherms for a) bulk and b) nanocrystalline Pd-H at 333 K measured in a Sievert's apparatus and in an *in-situ* hydrogen environment chamber.

enthalpies and entropies of formation for Pd-H to calculate that an increase in temperature of only 4 K accounts for the observed pressure difference.[1, 2]

III. *IN-SITU* DIFFRACTION RESULTS

A complete set of diffraction patterns corresponding to the in-situ isotherms (second cycle) of Fig. 3 are plotted in Figs. 4, 5 below. The color of each diffraction pattern corresponds to the total hydrogen content at each step in the isotherm.

The diffraction patterns were refined to extract lattice parameters as a function of hydro-

gen concentration, as described in the main text. The variation of lattice parameter with concentration was used to identify the phase boundaries in bulk PdH, as there is an abrupt change between single- and two-phase regions. For nanocrystalline PdH, we also refined the phase fraction, and report the fraction of the α-phase as a function of concentration in Fig. 6. The α- and β-phase boundaries are identified as the hydrogen concentration at which the α-phase fraction deviates from 1.0 (absorption) or 0.0 (desorption), respectively.

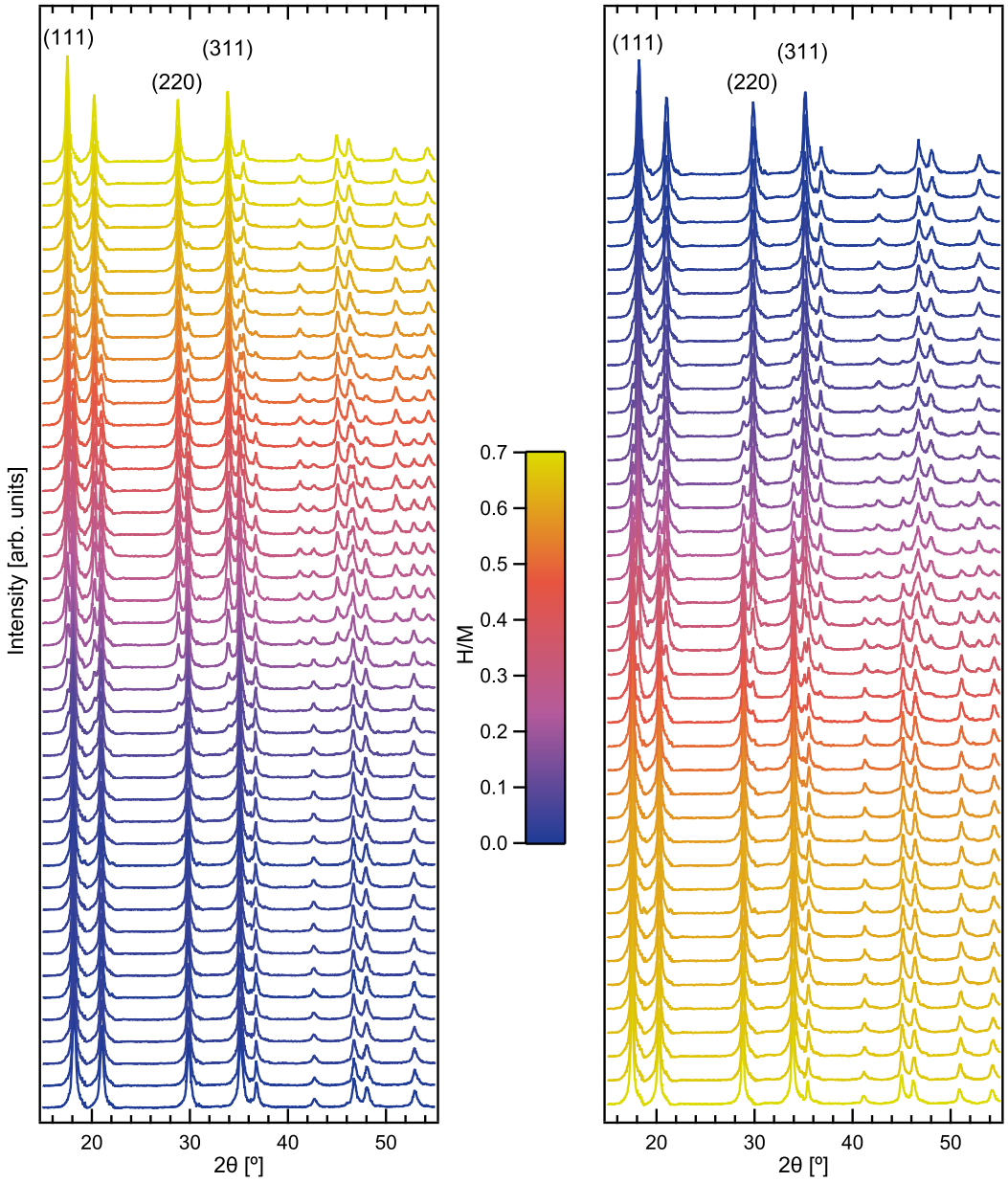

FIG. 4. *In-situ* X-ray diffraction patterns acquired during absorption (left) and desorption (right) by bulk Pd powder. The color of each trace corresponds to the total hydrogen content (in H/M) as indicated by the central legend.

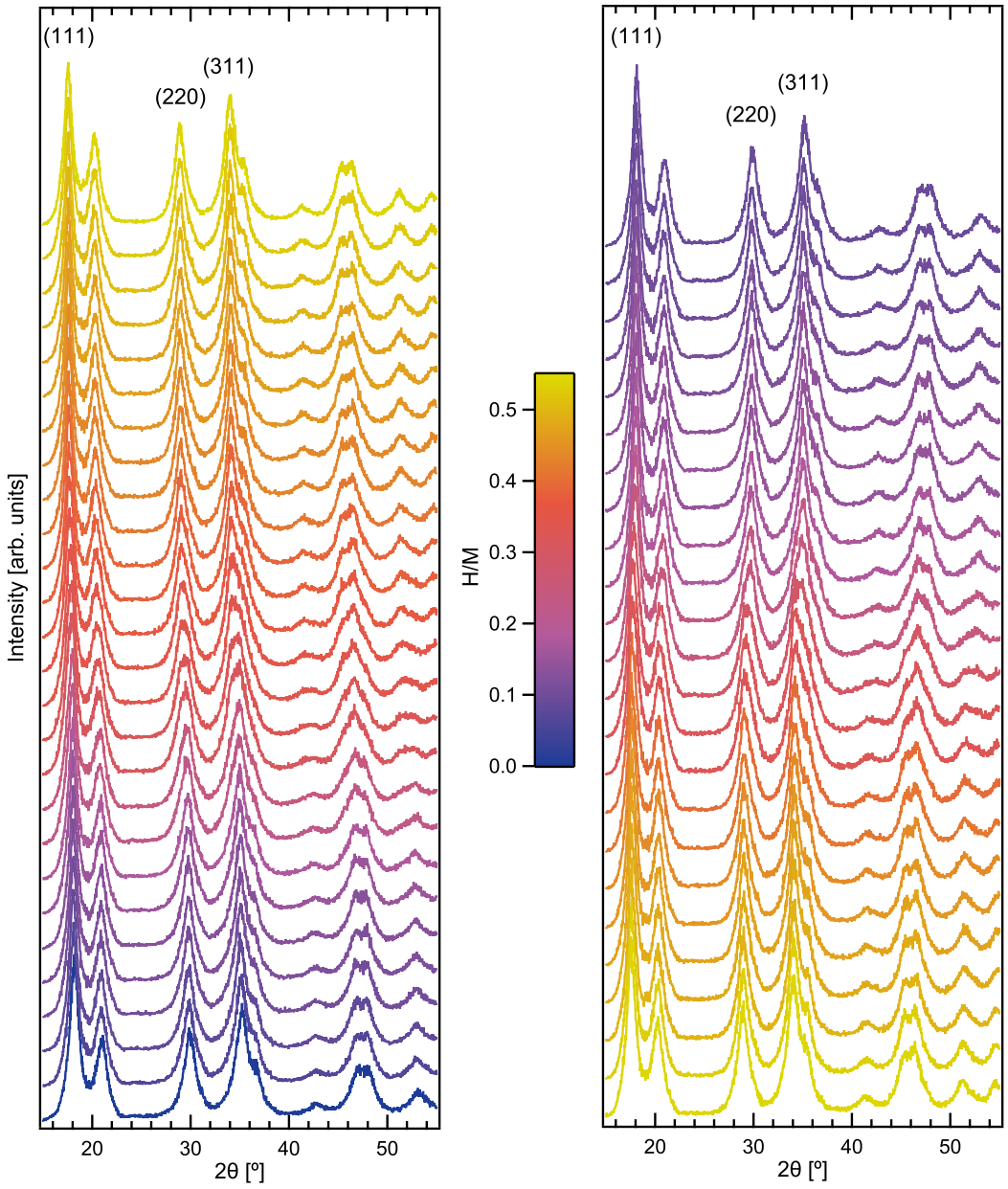

FIG. 5. *In-situ* X-ray diffraction patterns acquired during absorption (left) and desorption (right) by nanocrystalline Pd powder. The color of each trace corresponds to the total hydrogen content (in H/M) as indicated by the central legend.

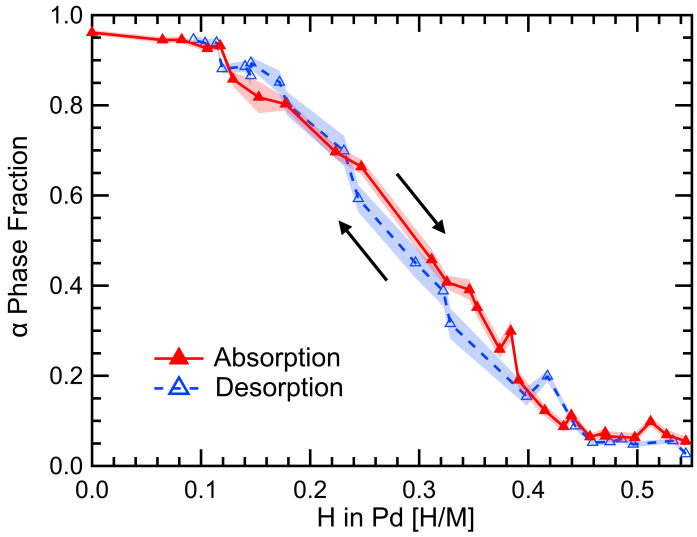

FIG. 6. Refined α-phase fraction during *in situ* absorption and desorption of hydrogen by nanocrystalline Pd. The black arrows indicate the direction of transformation, and shading around the traces correspond to the error bars.

IV. INTERFACIAL VELOCITY AND PRESSURE DECAY

Assuming that the departure from the equilibrium concentrations are small, the chemical potentials can expanded about the equilibrium, stress-free, states of both phases,

$$\begin{aligned} \mu_v^i(c) &= \mu_v^i(c_e) - c_e^i G_m''(c^i - c_e^i) \\ \mu_H^i(c) &= \mu_H^i(c_e) + (1 - c_e^i) G_m''(c^i - c_e^i) \end{aligned} \tag{1}$$

where $i = \alpha, \beta$. Using these in Eq. 11, with $[\![\xi]\!] \triangleq \xi^\beta - \xi^\alpha$ for a quantity ξ,

$$\rho_o [\![G_m''(1+B)(c - c_e)]\!] = -\eta Y e_e \tag{2}$$

Substituting these into the equation for the interfacial velocity equation, Eq. 10,

$$\begin{aligned} v = M\rho_0 \{ &[\![G_m''(1+B)(c-c_e)]\!] - \\ &Y e_{\mathrm{e}}^2 + 2\eta e_{\mathrm{e}} Y c_{\mathrm{e}}^\beta - \partial\phi_{\mathrm{p}}/\partial x \} \end{aligned} \tag{3}$$

Setting $v = 0$ in Eq. (3) and using Eq. (2) yields two linear equations for the unknown compositions c_p^β and c_p^α.

To determine the velocity after an aliquot of H has been added we use the expression for c_p^β and c_p^α in Eq. (2) and Eq. (3), these equations become,

$$[\![G_m''(1+B)(c-c_p)]\!] = 0 \tag{4}$$

$$v = \rho_0 M [\![G_m''(1+B)(c-c_p)]\!] \tag{5}$$

Using Eq. (4) in Eq. (5) to eliminate $(c^\beta - c_p^\beta)$, yields Eq. 23 of the main text,

$$v = \rho_0 M [\![c_p]\!] G_m''^\alpha (1+B^\alpha)(c^\alpha - c_p^\alpha) \tag{6}$$

Note the interfacial velocity does not depend on whether we consider the concentration at the interface in the α or β phases that due to Eq. (4).

Since the alloy concentration is constant after the aliquot of H has been added, the time derivative of Eq. 28 is,

$$0 = \frac{dc^\alpha}{dt} + \frac{d[\![c]\!]}{dt} f + [\![c]\!] \frac{df}{dt} \tag{7}$$

This equation should be written to first order in $c - c_p$ to be consistent the linearization of the thermodynamic terms in the local equilibrium and velocity equations. Since $[\![c]\!] = [\![c-c_p]\!] + [\![c_p]\!]$, $df/dt \sim [\![c-c_p]\!]$, and $f(t) = f_o + (df/dt)t$, where f_o is the initial volume fraction, to lowest order

$$0 = \frac{dc^\alpha}{dt} + \frac{d[\![c]\!]}{dt} f_o + [\![c_p]\!] \frac{df}{dt} \tag{8}$$

Using the local equilibrium condition, Eq. (4),

$$[\![c]\!] = \left(\frac{G_m''^\alpha (1+B^\alpha)}{G_m''^\beta (1+B^\beta)} - 1 \right) (c^\alpha - c_p^\alpha) + [\![c_p]\!] \tag{9}$$

Taking the time derivative on Eq. (9) and using this in Eq. (8),

$$0 = \frac{dc^\alpha}{dt} + f_o \left(\frac{G_m''^\alpha (1+B^\alpha)}{G_m''^\beta (1+B^\beta)} - 1 \right) \frac{dc^\alpha}{dt} + [\![c_p]\!] \frac{df}{dt} \tag{10}$$

Thus mass conservation implies,

$$0 = \left\{ \frac{G_m''^\beta (1+B^\beta)(1-f_o) + G_m''^\alpha (1+B^\alpha) f_o}{G_m''^\beta (1+B^\beta)} \right\} \frac{dc^\alpha}{dt} + [\![c_p]\!] \frac{df}{dt} \tag{11}$$

Which involves volume-fraction-weighted curvatures of the free energies in $B^i = 0$ limit. Thus,

$$\frac{dc^\alpha}{dt} = - \frac{G_m''^\beta (1+B^\beta) [\![c_p]\!]}{G_m''^\beta (1+B^\beta)(1-f_o) + G_m''^\alpha (1+B^\alpha) f_o} \frac{df}{dt} \tag{12}$$

which is Eq. 29 of the main text.

V. INTERFACE VELOCITY ESTIMATION

We can estimate the interface velocity from Equation (23) of the main text in the case of $B^\alpha = B^\beta = B$ and $G''^\alpha_m = G''^\beta_m = G''_m$. Then, Equation (23) can be rewritten as:

$$v = \tilde{M}(c^\alpha - c^\alpha_p) \tag{13}$$

where $\tilde{M} = \rho_0 M G''_m (1+B)[\![c_e]\!]$. Using this approximation, we determine the pressure equilibration as outlined in the main text Section II.D. Equation (34) of the main text becomes:

$$P(t) = P_\mathrm{p} + P_\delta \exp\left\{-[\![c_\mathrm{e}]\!]\tilde{M} S_V(f) t\right\} \tag{14}$$

where P_p is the pinning pressure and the transient pressure excursion is $P_\delta = [\rho_0(c^\alpha_\mathrm{pi} - c^\alpha_\mathrm{p})(1+B)G''_m P_\mathrm{p}]/[k_B T]$. To place bounds on the range of v, $S_V(f)$ is calculated for two geometries; a half-transformed particle with an equitorial disc as the interface, and a particle with several discs $1.5\,\mu$m in diameter and 50 nm thick (corresponding to $f = 0.035$), as observed by Ho, et al.[3]. They measured an interfacial velocity of $2.1 \times 10^{-3} \mu$m/s at 90 K, placing a lower bound on $\tilde{M}$ for our system. For a given $S_V(f)$ and $\tilde{M}$, the velocity varies with hydrogen aliquot size according to Eq. 13. A maximum velocity is assumed for $c^\alpha - c^\alpha_p \approx 0.7$, which decays to approximately 1 nm/s before the interface stops. The range of maximum interface velocities for various $S_V(f)$, derived from the experimentally measured equilibration times τ, is plotted in Fig. 7.

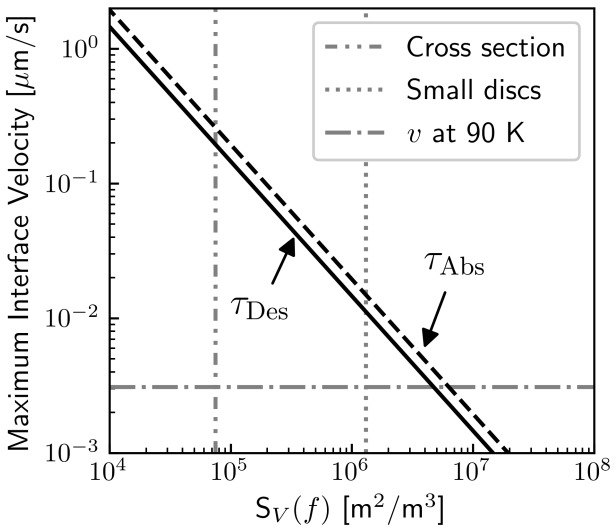

FIG. 7. Maximum interface velocity as a function of surface area per volume as determined from τ, Eq. 13 and the exponential in Eq. 14. The dashed vertical line corresponds to S_V of a half-transformed sphere, and the dash-dot-dot line corresponds to S_V of several disc-shaped precipitates. The horizontal dash-dot line is the measured velocity at 90 K by Ho, et al.[3]

[1] G. Sandrock, A panoramic overview of hydrogen storage alloys from a gas reaction point of view, **293–295**, 877.

[2] R. Lässer and K. H. Klatt, Solubility of hydrogen isotopes in palladium, Physical Review B **28**, 748 (1983).

[3] E. Ho, H. Goldberg, G. Weatherly, and F. Manchester, An in situ electron microscope study of precipitation in palladium-hydrogen alloys, Acta Metallurgica **27**, 841 (1979).